Free-Carbon Surface for PtCu Nanoparticles: an *in situ* NAPXPS Study

Rafael Castillo[†§*], Sara Navarro-Jaén[†], Francisca Romero-Sarria[†], Virginia Pérez-Dieste[‡], Carlos Escudero[‡], Miguel Ángel Centeno[†], Marco Daturi[§], José Antonio Odriozola[†*].

[†] Inorganic Chemistry department, University of Seville and Institute of Material Science of Seville (US-CSIC), 41092 Seville, Spain.

[§] Normandie Univ, ENSICAEN, UNICAEN, CNRS, Laboratoire Catalyse et Spectrochimie, 14000 Caen, France.

[‡]ALBA Synchrotron Light Source, Carrer de la Llum 2-26, 08290 Cerdanyola del Vallès, Barcelona, Spain

[*]Corresponding authors: rcastillo4@us.es, odrio@us.es

KEYWORDS: Platinum, Copper, nanoparticles, PVP removal, carbon overlayers, CO-PROX, in situ spectroscopy, NAPXPS.

ABSTRACT

Usually, nanoparticles synthesis methodologies require the use of organic molecules (capping agent, solvent molecules, etc) which results in carbon deposits on

the nanoparticles surface. These residues modify the surface properties mainly affecting to the catalytic behavior. In this work, unsupported poly(vinylpyrrolidone) (PVP)-stabilized PtCu (1:3 molar ratio) bimetallic alloy nanoparticles were synthetized and characterized. An alternative surface cleaning method has been designed which successfully removes the presence of organic fragments. To address this key issue, we have combined a first nanoparticles washing step with a near ambient pressure X-ray photoelectron spectroscopy (NAPXPS) study in order to obtain a clean active site and the total understanding of the carbon elimination mechanism. The dynamic evolution of the surface organic species composition under different gas mixtures at 750 mTorr and 350 ºC has been studied, and only under CO_2 exposure, NAPXPS analysis revealed a total availability of the active site by the removal of the organic nanoparticle coating.

KEYWORDS: Platinum, Copper, Nanoparticles, NAPXPS, Capping agent removal.

1. INTRODUCTION

Many industrial catalysts are typically formed by highly dispersed metal species on an inert support. In general, these nanoparticles present irregular shapes and a relatively wide particle size distribution. As catalytic processes occur at the nanoparticle surfaces, their size and shape strongly influence the catalytic activity since the number and nature of undercoordinated atoms clearly depends on these parameters. Moreover, the geometrical and electronic structure of surfaces determines the interaction of adsorbates with the catalyst surface.

Metallic nanoparticles (NPs) are usually synthesized from salts solutions containing the metal of interest [1–4]. Roucoux *et al.*[5] provided a comprehensive review on synthetic methods of colloidal nanoparticles. Most methods consider the use of strong reducing agents and capping ligands and/or structuring molecules for stabilizing the colloids. However, adsorbed capping agents, structuring molecules and/or the reducing

agents and their oxidized counterparts, although seldom studied, may modify the nanoparticle surface sites thus affecting their catalytic [6].

Baker et al.[7] studied PVP and oleic acid (OA) capped Pt NPs. These authors found that the presence of the capping agent does not inhibit the catalytic process in the hydrogenation of ethylene or the oxidation of methanol but the clean surfaces are only active in the hydrogenation of ethylene. On the other hand, Park et al.[8] found by partially removing the capping layer that the catalytic activity increases but the activation energy remains unaltered pointing to a platinum surface site blocked by the capping molecules or carbonaceous rests on the nanoparticles surface. Moreover, they showed that the nature of the capping molecule affects the catalytic activity for CO oxidation while keeping constant the activation energy, which again points to a blocking phenomenon. UV-ozone cleaning is attempted by these authors to elucidate the role of the adsorbed overlayers. This treatment results in the oxidation of the Pt surface that raises some questions on the effect of oxidized sites on the catalytic activity for CO oxidation. In addition, the blocking phenomenon may favor the catalyst performances as reported for benzyl alcohol oxidation in the presence of PVA (poly(1-acetyloxiethene) due to the preferential blocking of Pd(111) sites [9].

The removal of the overlayers generated during the nanoparticles synthesis procedure is not an easy task. Lopez-Sanchez *et al.*[10] stressed the difficulty in removing capping agents that they claim can only be completely removed using oxidative treatments. These authors state the significant conversion decrease on the catalytic activity of PVA-stabilized Au/TiO_2 catalysts for CO oxidation. Therefore, strongly adsorbed capping agents may block the access of reactant molecules to the nanoparticles surface lowering their activity. Zhong *et al.*[1] proposed an ultraviolet-ozone (UVO) treatment to remove the residues that ensures the elimination of the stabilizer and their carboxylate-derived oxidation products after prolonged periods of time (> 12 h). However, for some reactions the presence of PVP residues seems to improve the catalytic behavior of Au nanoparticles.

Although some authors argue that the capping agent can be successfully removed without oxidative treatments, the presence of vibrational modes associated to the capping agent in Raman and FTIR spectra of the nanoparticles surface after their cleaning procedure raises serious doubts on the effectiveness of their removing process[11]. However, a new question may be raised at this point: may the presence of carbon overlayers on the surface of the nanoparticles tailor their catalytic properties?

The role of carbon fragments on the catalytic activity of alumina supported Pt or PtCu bimetallic catalysts has also been evidenced in the preferential oxidation of CO (CO-PROX reaction). [12]. The decomposition of acetate ions, added to favor Pt dispersion, results in the formation of carbon overlayers that modulate the catalyst activity and selectivity. The activation atmosphere of the PtCu catalysts strongly influences its catalytic activity. Various possibilities are envisaged by Romero-Sarria *et al.*[12] for explaining this observation; different atmospheres result in different carbon coverages or second, the activation atmosphere results in a different surface composition of the metal, or a combination of both. By operando IR-MS spectroscopy the influence of the presence of surface CH species as a function of the activation treatments is evidenced. The shift observed for the linear form of adsorbed CO on platinum indicates that these surface species alter the surface electron density of the metallic sites and hence the catalytic activity.

However, systematic studies on the effects of possible coatings resulting from the synthesis process are not always considered. For instance, M. Cargnello et al. [13] show how a fast thermal treatment can remove ligands without modifying structure and composition of supported nanocrystals. Also, Alayoglu *et al.*[14] synthesized Ru@Pt core-shell and RuPt NPs for testing the effect of alloying in the preferential oxidation of CO. These authors used the polyol method for reducing the $Ru(acac)_3$ precursor in presence of PVP. The obtained particles are further coated with $PtCl_2$, which results in core-shell nanoparticles. They employed the same method for the synthesis of bimetallic PtRu nanoparticles but using $[Ru(CO)_3Cl_2]_2$ and $Pt(acac)_2$. The nanoparticles were

activated in H_2 at 200ºC prior to the PrOx reaction. Although a final heating step at 500ºC for the bimetallic catalyst is considered, in general, the activation treatment based on oxidation, H_2-reduction and/or activations in the reaction atmosphere to eliminate the hydrocarbon molecules may modify the surface of the synthesized nanoparticles by changing their composition. In this sense, Zhan *et al.*[15] synthesize AuCu NPs and use the oxophilicity of copper for generating a structured Au/CuO_x catalyst since Cu selectively segregates to the surface under oxygen atmosphere, a technology, on the other hand, early discovered by prehispanic cultures in South America[16].

In this sense, PtCu based catalysts are one of the most studied systems for CO-PROX reaction because their high activity/selectivity balance and their good performance in a wide temperature range[17,18]. However, the catalyst structure and surface composition remains unclear. In a previous study[12], we have shown a strong dependence of the activation temperature, the nature of the conditioning atmosphere and the heating rate during the activation on the CO conversion. The best catalysts were obtained when conditioning the catalysts in the Water-Gas Shift reaction (WGS) surrogate outgas flow at low temperatures using moderate rates for heating to the maximum activation temperature. Two main hypotheses were raised on analyzing these data: the existence of complex redox processes occurring during the activation that result in adsorbed carbonaceous species with their coverage depending on the activation procedure, and/or the surface restructuring that results in differences in composition as a function of the activation parameters[12].

To understand the role of Pt and Cu in this reaction, well-defined PtCu model nanoparticles are synthesized and the nature of the resulting surface composition is studied by NAPXPS as a function of different components of the surrogate reforming gas.

2. EXPERIMENTAL

2.1. Synthesis of $PtCu_3$ NPs.

Taylor *et al.*[2] developed a synthesis procedure to obtain Pt_3Cu nanodendrites. This method is based in a two-step reduction process that uses a slow kinetic reduction in the first step followed by a fast reduction employing ascorbic acid. However, this synthesis procedure is unable to synthesize PtCu or $PtCu_3$ nanoparticles. A modification of this procedure allows the control of size and composition of $PtCu_3$ nanoparticles. Briefly, 25 mL of ethylene glycol (99% for synthesis) (EG) were heated at 110 ºC for 1h. Then, 4 mL of $H_2PtCl_6 \cdot xH_2O$ and 12 mL of $CuCl_2 \cdot 2H_2O$, as precursors, and 8 mL of PVP (M_w=55000), as capping agent, (1:1:1 molar ratio) were simultaneously added. In all cases, ethylene glycol was used as solvent. The mixture was held at 110 ºC for 2 hours. At this point, a $NaBH_4$ (3M) solution was added dropwise under vigorous stirring and the mixture was kept for 15 minutes. The product was subsequently washed with acetone allowing the nanoparticle precipitation. The resulting solid was dried at 80 ºC overnight.

2.2. Characterization.

To get information on the structure and composition of the obtained nanoparticles, X-ray diffraction (XRD) was performed on a high-temperature Philips X'Pert Pro diffractometer. Diffraction patterns were recorded using Cu Kα radiation (40 mA, 45 kV) over 2θ range of 5° - 90° and a position-sensitive detector using 0.05° step size and 1200 s step time. XRD data were acquired at room temperature, 220 ºC and 350 ºC. The temperature heating rate was 10 ºC/min. International Centre for Diffraction Data (ICDD) was used as XRD database.

The nanoparticles morphology and size were studied by high-resolution transmission electronic microscopy (HRTEM) by averaging over 200 particles on a 200kV JEOL JEM-2010F instrument with a structural resolution of 0.19 nm at Scherzer defocus conditions. To avoid the carbon contribution, samples were deposited directly onto Ni grids.

Ultraviolet-visible spectroscopy (UV-VIS) was carried out in an Avantes AvaLight-DH-S-BAL spectrophotometer equipped with an optic fiber liquid sensor for wavelengths from 100 to 1000 nm.

Near ambient pressure X-Ray photoelectron spectroscopy (NAPXPS) experiments have been performed at the NAPP instrument installed at the CIRCE beamline from the ALBA Synchrotron Light Source (Barcelona, Spain)[19]. N1APXPS measurements were carried out using a PHOIBOS 150 NAP SPECS analyzer equipped with four differentially pumped stages. The beam spot size at sample was approximately 100 x 125 μm^2 (HxV). The spectra were acquired with 20 eV of pass energy and 0.05 eV kinetic energy step. The work pressure was 750 mTorr for all the different gas atmospheres used. The kinetic energy for all the measured photoelectrons was around 170 eV and the energies were referred to the Fermi level. For the estimation of IMFP (Inelastic mean free path) , we employed the TPP-2M formula proposed by Tanuma *et al.*[20] considering a closed $PtCu_3$ alloy (density of 12.08 g/cm^3 and 43 valence electrons per molecule). Consequently, the IMFP for the photon energies employed is around 0.45 nm. The composition of the gas mixture dosed into the analysis chamber was defined by Mass Flow Controller.

3. RESULTS AND DISCUSSION

3.1. Nanoparticles structure

XRD pattern of the synthesized nanoparticles showed diffraction peaks corresponding to a Pt-Cu bimetallic alloy with a face-centered cubic (fcc) structure and a composition close to the targeted 1:3 Pt:Cu atomic ratio [21] (see supplementary data). Considering this structure and the observed diffractions lines, the calculated lattice parameter for the obtained Pt-Cu alloy is 3.721Å, slightly larger than the one reported for the $PtCu_3$ intermetallic compound (3.702Å) (JCPDS #00-035-1358).

Assuming a disordered fcc lattice for the Pt-Cu alloy, an estimation of the atomic composition using Vegard's law results in a 33:66 Pt:Cu atomic ratio. However, the

binary Pt-Cu phase diagram is quite complex in this compositional range and at the same time the two step reduction process may result in a “nano-onion” type structure resulting in a well-defined core structure and a surface layer of smaller thickness[5]. Therefore, a core particle with a composition slightly departing from the desired one surrounded by a Cu-rich outer layer may be assumed.

For avoiding agglomerates, which prevent the morphological study of the nanoparticles, $PtCu_3$ nanoparticles were supported on α-Al_2O_3. The high crystallinity degree of the support and the extremely low specific surface (around 8 m^2/g) facilitate the morphological study by HRTEM. Micrographs reveal a monomodal sharp size distribution of nanoparticles with an almost circular projection, which allows estimating an average diameter of 2.7 ± 0.6 nm (Figure S2, supporting information).

3.2. Surface Cleaning Method Development.

The obtained nanoparticles may have capping agents/carbonaceous residues and other trace elements from the reducing agents on their surface. High Angle Annular Darkfield Scanning Transmission Electron Microscopy (HAADF-STEM) mode, which allows the study of metallic nanoparticles supported in low-Z atoms (Figure 1) was applied. At the same time, EDS analysis was carried out. The analysis reveals an homogenous distribution of platinum and copper on the support as well as the presence of carbon deposits associated to the PtCu metallic phase.

Therefore, a careful study of the presence of these overlayers and the procedures to remove them trying to avoid any alteration of the nanoparticle size and shape was carried out. First at all, thermal desorption experiments were considered, since they allow to detect the presence of these capping/solvent molecules on the nanoparticle surface.

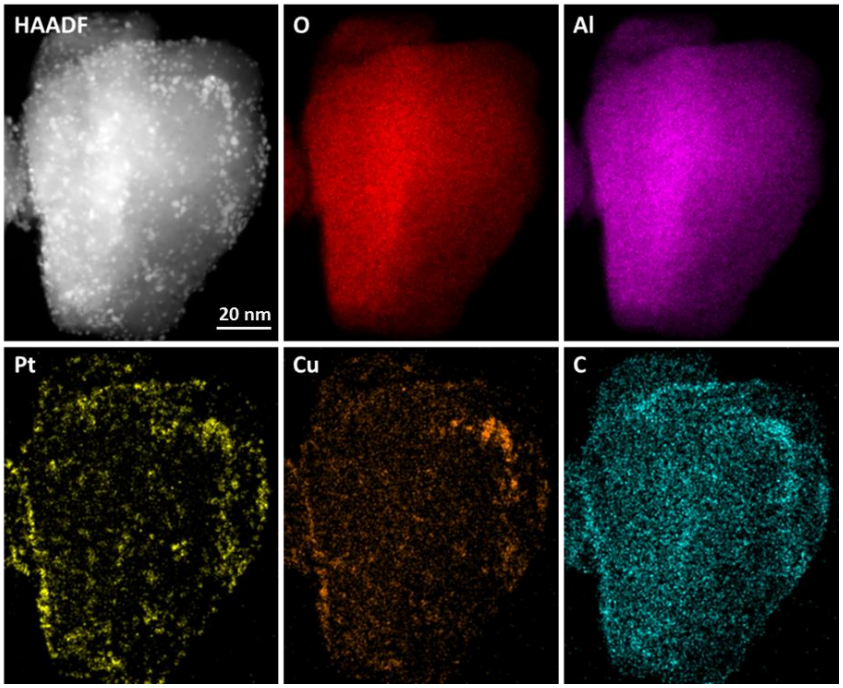

Figure 1. HAADF-STEM image of $PtCu_3$ nanoparticles supported on $\alpha - Al_2O_3$ and elemental map of each single element.

The decomposition of PVP (capping molecules) is catalyzed by Pt that reduces its decomposition temperature[22] down to 350 ºC; moreover, in the presence of Pt, the PVP degradation accounts just for ca. 69% weight loss while pure PVP decomposes almost completely (>95% weight loss referred to the initial PVP mass). Although the main mechanism for decomposition is assumed to be depolymerization, the formation of amorphous carbon remaining on the Pt surface has been reported by Borodko *et al.*[23] accounting for the differences in the decomposition degree.

Mass spectrometric analysis of the evolved gases reveals a complex decomposition pattern for the molecules remaining at the nanoparticle surface. For the sake of simplicity just mass-to-charge 16, 18, 28, 41 and 44 ratios are plotted in Figure 2. These m/z ratios are assigned to the evolution of methane, water, carbon monoxide, methyl isocyanide (a product of the reduction of PVP) and carbon dioxide.

The observed profiles with significant gas evolution of CO and methylsocyanate at 300 and 450 ºC account for PVP decomposition. The low temperature evolution of H_2O and CO_2 may be indicative of the presence of ethylene glycol molecules on the

nanoparticle surface. Gas evolution is observed at temperatures as high as 800 ºC, indicating that not only amorphous carbon, but organic fragments remain on the surface and this demonstrates the presence of at least the capping molecule on the nanoparticle surface. Thermal treatments at these high temperatures should result in nanoparticle sintering and must be discarded[24].

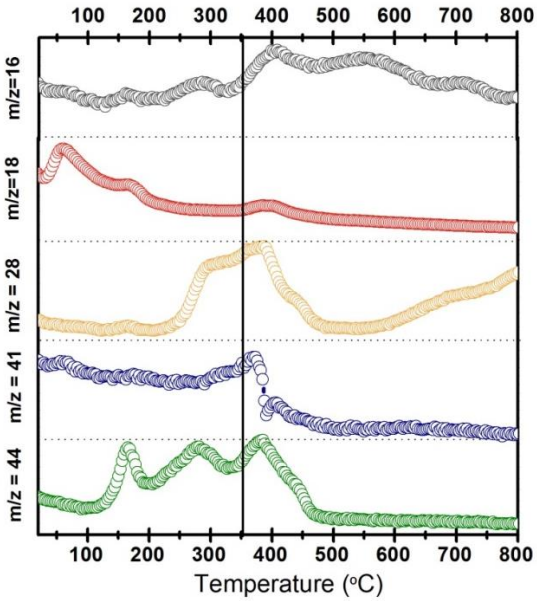

Figure 2. Temperature programmed desorption – mass spectroscopy in 50 mL/min Ar flow of $PtCu_3$ from room temperature to 800 ºC (10 ºC/min). The solid line indicates the usual temperature for the beginning of the nanoparticles sintering phenomenon. As it can be seen, under these conditions the amount of remaining surface species cannot be neglected.

Low temperature air calcination of nanoparticles was attempted to get nanoparticles free of carbonaceous residues. Figure 3 shows selected *in situ* XRD patterns of $PtCu_3$ nanoparticles during heating the nanoparticles in an O_2-rich atmosphere from RT to 350 ºC. A dealloying process is clearly observed upon the oxidizing treatment at high temperatures. At 220 ºC copper segregation takes place, resulting in oxidized copper species (monoclinic CuO phase with a C2/c symmetry) and $Pt_xCu_{1-x}O$ species (tetragonal phase with a $P4_2/mmc$ symmetry)[25]. At 350 ºC the PtCu nanoparticles are completely dealloyed to metallic platinum and oxygen-containing copper phases (CuO and $Pt_xCu_{1-x}O$).

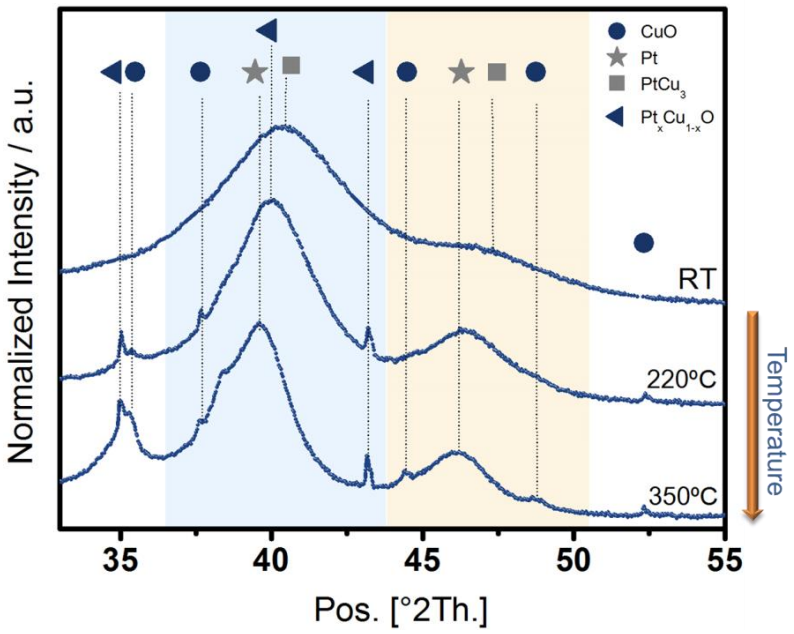

Figure 3. *In situ*-XRD data of $PtCu_3$ nanoparticles obtained under O_2- rich atmosphere. XRD data was taken at room temperature, 220 ºC and 350 ºC.

It is clear that the mild oxidation treatment to remove carbon contamination results in the segregation of the alloyed metals to metallic platinum, oxidized copper species and a new $Pt_xCu_{1-x}O$ solid solution phase where x may vary from 0.135 to 0.355)[25]. The nature of the segregated phases was analyzed by peak deconvolution. The analysis reveals that the obtained metallic platinum phase is highly crystalline and also, a remarkable growth of the particle size, especially of the oxidized copper species (20 nm).

An alternative procedure has been developed to avoid dealloying and to remove the capping PVP molecules as well as solvent and organic molecules that may be formed during the redox processes. The procedure is based on exchanging the PVP ligands, at room temperature, with thermodynamically more stable ones that, at the same time, may be easily decomposed/removed at low temperatures. The developed method consists of an exchanging step, taking advantage of the quelate effect, using a mixture of acetic acid (a bidentate ligand), water and acetone. In this sense, prior to the conditioning process, 40 mg of the PVP-protected nanoparticles were added to 10 mL of a ~2 mM acetic acid solution under vigorous stirring for 10 minutes, then the nanoparticles were precipitated

by adding acetone and further separated by centrifugation. This step was repeated until the presence of PVP was not detected by UV-Vis in the remaining solution.

Figure 4 presents the spectra of three consecutive washing experiments together with the spectra of pure PVP and acetic acid diluted on EG solutions. The PVP absorption spectrum shows a band with a maximum at 242 nm assigned to the π→ π* electronic transition of C=O and C=C groups of the PVP molecules.[23]. Upon three washing cycles, the main band at 242 nm shifts to lower wavelengths (234 nm). The band characteristic of the acetic acid aqueous solution also appears at 234 nm.[26] This may indicate either that the PVP has been completely removed and exchanged by acetate species or that the remaining PVP cannot be further removed by this method.

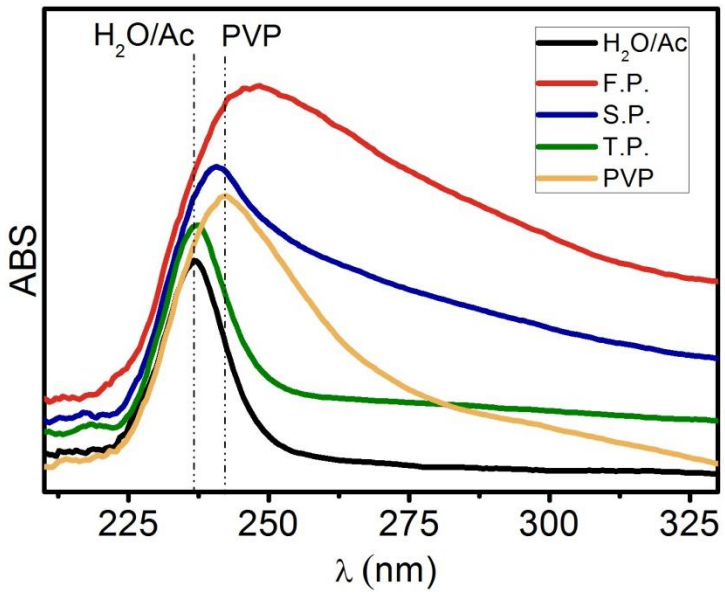

Figure 4. UV-Vis spectra of $PtCu_3$ nanoparticles cleaning liquid after different purification steps; acetic acid solution (black), PVP solution (yellow), supernatant after first (red), second (blue) and third purification (green) steps.

To prove this, a new temperature programmed desorption – mass spectroscopy (TPD-MS) was carried out on these acetic acid-treated nanoparticles. The characteristic m/z=41 of the PVP molecules is no longer present indicating that PVP is successfully removed (See supporting information). However, gas evolution is compatible with the presence of acetates adsorbed on the metal surface.

The presence of surface acetate species may also influence the nature of the nanoparticle surface. Thermal decomposition of adsorbed acetates may occur through dehydration to ketene that rapidly transforms leading behind surface carbon[12,27].To test this hypothesis the surface of the nanoparticles was analyzed by near ambient pressure x-ray photoelectron spectroscopy (NAPXPS). The presence of a remarkable carbon signal is evident (Figure 5). A typical gas stream surrogate entering the CO-PROX reactor may be described as H_2:CO_2:CO:H_2O 60:15:1:24. For understanding the catalyst surface behavior under the actual activation step of the industrial catalysts[28], the nanoparticle surface was submitted to a consecutive series of treatments modelling the actual gas streams in the NAPXPS instrument. This sequence does not modify the size and shape of the nanoparticles as determined by TEM (See supporting information).

Self-supported nanoparticle pellets were submitted to different gaseous environments at 750 mTorr while keeping the sample holder temperature at 350 ºC. Consecutive treatments of the fresh sample under these conditions were performed changing the model reactive atmospheres from vacuum to H_2, H_2:H_2O 1:1, CO_2, H_2 and CO_2:H_2 2:3. Once stabilized the surface of the nanoparticles under the different atmospheres, C 1*s* and O 1*s* high resolution spectra were recorded. The C 1*s* signal only disappears completely under a flow of CO_2, thus indicating the removal of the surface carbon (Figure 5).

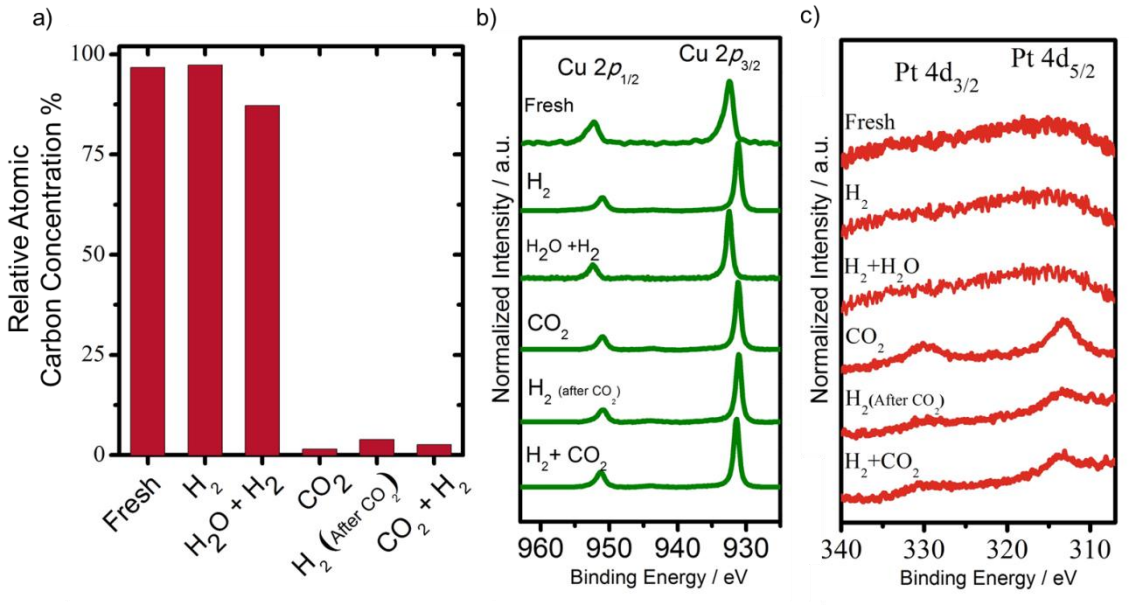

Figure 5.a) Relative surface amount of carbon estimated from NAPXPS spectra as a function of the activation treatment. **b)** Cu (2*p*) core-level NAPXPS spectra under different *in situ* treatments; vacuum, 750 mTorr H_2, 750 mTorr H_2+H_2O (1:1), 750 mTorr CO_2, 750 mTorr H_2 (after CO_2 treatment), 750 mTorr CO_2 and H_2 (2:3). **c)** Pt (4*d*) core-level NAPXPS spectra under different *in situ* treatments. Incident photon energy is 1100 eV for Cu (2*p*) and 485 eV for Pt (4*d*).

One of the relevant aspects to be studied is the effect of the new *in-situ* treatment for removing the surface carbon on the nature of the metallic surface species. It is clear that whatever the treatment the Cu 2*p* spectrum does not show any satellite peak (Figure 5.b). This absolutely discards the existence of Cu^{2+} species on the nanoparticle surface for all the tried treatments. However, a shift in the Cu 2*p* binding energy may be observed as a function of the gaseous environments that might be associated to a modification of the atomic relaxation energy since a modification of the copper environment[29] .

The combination of the shape and binding energy of Cu 2*p* photoelectrons together with the shape and energy position of the $L_3M_{4,5}M_{4,5}$ Auger lines of copper allows identify the oxidation state of copper[30,31]. Cu (II) bulk oxides are characterized by large satellite peaks at binding energy ca. 9 eV of the main photoelectron peak. These satellites are not present in metallic copper or Cu_2O that are hardly differentiated on the basis of their Cu 2*p* binding energies. However, these two copper species may be differentiated by analyzing their X-ray excited Auger spectra since the $L_3M_{4,5}M_{4,5}$ Auger

lines since the kinetic energies of Cu (I) and Cu(0) differs by ca. 2 eV, being higher the one corresponding to metallic copper[32]. However, the shape and position of these signals depends, among other factors, on the particle size of the analyzed phases and, when supported, on the electronic properties of the support[33].

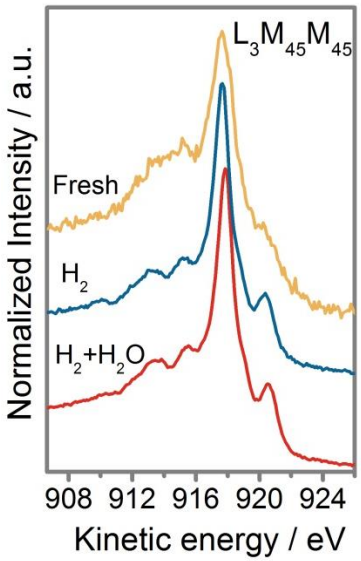

Figure 6. $L_3M_{4,5}M_{4,5}$ Auger spectra of copper as a function of the activation treatment.

The Auger spectra are independent of the treatment and characterized by lines at 920.5, 917.8, 915.1 and 913.4 eV being the most intense one ascribed to the ^1G term arising from the decay of the d^8 final state term[34–36]. In all cases the spectra show all the features typical of metallic copper Auger spectrum[32,37]. Therefore, the observed shift in the Cu(2*p*) binding energy upon exposure to the H_2+H_2O mixture cannot be ascribed to a modification of the copper oxidation state but to a modification of the atomic relaxation energy[29,33].

Comparing the Pt 4*d* peaks during the different treatments (figure 5.c), the Pt 4*d* signal is hardly appreciable until the surface is submitted to a CO_2 atmosphere and carbon concentration is dramatically reduced indicating that the carbon overlayer has been completely removed with the CO_2 treatment, improving thus the platinum availability as active site. Hydrogen addition to the CO_2 flow results in an increase of the

carbon amount that buries platinum atoms and therefore reduces the intensity of the Pt (4*d*) signal.

Figures 7 and 8 present the O 1*s* and C 1*s* XP spectra under different gaseous environments. For all the experimental conditions, a weak oxygen signal is always appreciable; however, no oxidation is detected for Cu or Pt.

In the fresh, H_2-treated and H_2+H_2O-treated samples the C 1*s* spectra closely resembles those of carbon materials including the tail at high binding energies (~290 eV) corresponding to the π→ π* transition shake-up present in graphitic or aromatic compounds (Figure 7). Careful subtraction of the different signals allows a tentative deconvolution of every spectrum considering the model of Lerf-Klinowski concerning highly oxidized graphitic structures[38]. According to this model, C 1s peaks at 285.4, 286.2, 287.0, 287.9, 288.9, and 290.4 eV assigned to C–C, C–O, C=O, O–C–O, O=C–OH and π→ π* transition in aromatic systems may be observed[39–41]. Obata *et al.* in their study on graphite and graphene oxide simplified the model considering the contributions from aromatic rings (C=C/C-C) at 284.5 eV, epoxy (C-O) at 286.8 eV, carbonyl groups (C=O) at 287.8 eV and carboxylic groups(-COOH) at 289.0 eV[42].

Signals corresponding to isolated carbon atoms (283.8 eV), adsorbed polymeric carbon (284.1 eV), graphene (284.4 eV) and aliphatic polymers (285.0) have been also described and assigned in literature[43].

Therefore, the fresh nanoparticles may be described as a PtCu alloy covered by a relatively thick graphitic and aliphatic composite layer slightly oxidized. The surface species in this sample correspond to graphitic-like species (284.6 eV) together with carbon sp^3 species, partially hydrogenated polymeric carbon (285.2 eV), and a small proportion of oxygenated species mainly C-O (286.2 eV) and C=O species (286.7 eV).

Upon hydrogenation (H_2-treated sample) carbon with sp^3 character increases their relative population but the thickness of the carbon overlayer is hardly altered. The relative proportion of surface oxygen species in the fresh and the H_2-treated samples is

very small although with a complex structure presenting. The H_2+H_2O mixture reduces the carbon with sp^3 character showing their higher reactivity towards H_2O resulting in an increase in the relative proportion of oxygenated species.

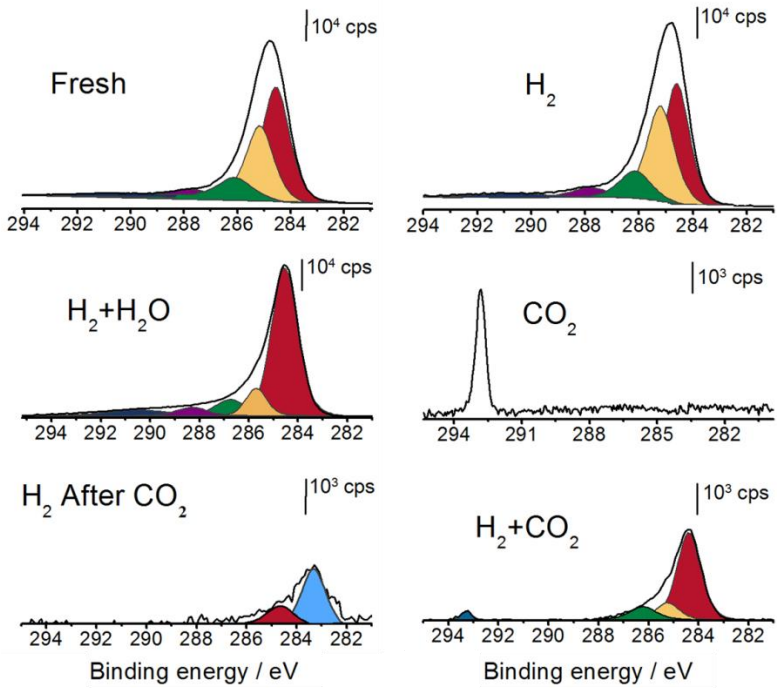

Figure 7. C 1*s* spectra from $PtCu_3$ nanoparticles under different gaseous environments. Characteristic contribution from isolated carbon atoms appears at 283.3 eV (dark green color). Peaks corresponding to graphitic carbon atoms with sp^2 and sp^3 hybridization are at 284.6 eV (dark cyan color) and 285.2 eV (grey color) respectively. Oxygenated species show characteristic peaks at 286.2 eV (wine color) and 286.6 eV (yellow color). Satellite peak at around 290.4 eV corresponds to π→ π* transitions in aromatic systems. Peak at around 292.7 eV corresponds to CO_2 gas phase.

The O 1*s* signal from the fresh sample exhibits a wide peak centered at 532.1 eV (Figure 8) that may be decomposed in four contributions: quinone-like groups at 530.9 eV (green trace), double-bonded oxygen to carbon at 531.5 eV (wine trace), single-bonded oxygen to carbon at 532.4 eV (gray trace) and adsorbed water at 533,4 eV (dark blue trace)[39,41,44]. The overall O 1*s* contribution at 531.8 eV is shifted 0.3 eV to lower binding energies with respect to the fresh sample. This is mainly due to the reduction of

the oxygen double-bonded to carbon (532.4 eV) forming reduced C-OH groups (531.5 eV), but the total C and O amount remains almost unaltered.

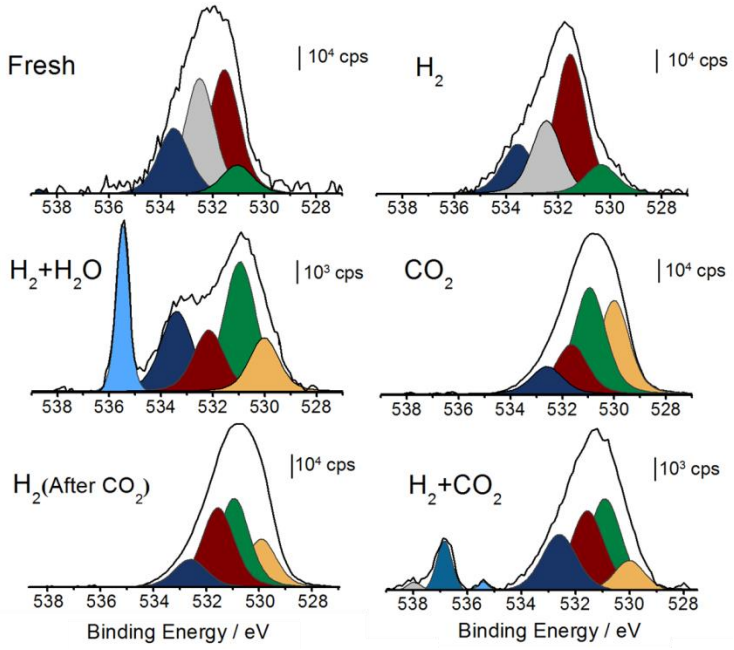

Figure 8. O 1*s* spectra from the $PtCu_3$ nanoparticles under different gaseous environments. At lower energies, we found peaks characteristic of atomic oxygen at 529.9 eV (orange color) and hydroxyl groups (O-H) at 530.9 eV (green color). Peaks arising from different contributions (oxygen from carbonyl groups, adsorbed electrophilic atomic oxygen and subsurface oxygen) have the maximum at 531.6 eV (wine color). The peaks around 532.5 eV correspond to oxygen single-bonded to carbon. Finally, contributions from adsorbed molecular water appear in the range between 532.5 and 533.4 eV (dark blue color) depending on the coverage degree. The gas phase peaks of H_2O, CO_2 and CO appear at 535.5 eV (sky blue color), 536.6 eV (blue color) and 537.7 eV (light gray color) respectively.

When exposing the samples to the H_2+H_2O atmosphere, the total amount of carbon decreases while the oxygen concentration increases. The main overall O 1*s* contribution shifts to even lower binding energies (530.9 eV) although a clear shoulder attributed to adsorbed water molecules appears at ~533.2 eV and there is also a sharp contribution at 535.5 eV corresponding to H_2O gas phase. This treatment results in the appearance of new components at 529.9 and 530.9 eV as well as to an increase in the concentration of the C=O and H_2O_{ads} components. Eren *et al.*[45] observed for methanol

adsorption on Cu (100) O 1*s* signals at 529.6, 531.1 and 534.0 eV ascribed to atomic oxygen, hydroxyl and adsorbed water, respectively. In the same report, the contributions at 532.2-532.4 and 531.4 eV are assigned to adsorbed methoxy and formate species, respectively. Similarly, for Ni/CeO_x (111) the O 1*s* binding energy of the adsorbed ethoxy species also appears at 532.3 eV[46].

The treatment under CO_2 gas results in an almost free carbon surface. Traces of carbon that might be associated to the presence of adsorbed CO species are insinuated at ~287 eV, in agreement with the presence of an O 1*s* signal at 532.7 eV (Figure 8). CO adsorbed on PtCu alloys only shows a single contribution in both the C 1*s* and O 1*s* XP spectra at 286.6 and 532.6 eV, respectively[47]. These values are consistent with previous reports for top CO adsorption on Pt (111), being the O 1*s* signal hardly shifted with respect to CO adsorbed on Pt(111)[47]. However, in CO chemisorption studies on Pt/Cu/Pt(111)[38] have been described O 1*s* contributions at 533.3 and 531.5 eV, corresponding to CO molecules adsorbed on top and bridge sites, at binding energies slightly higher than for the Pt(111) system. These authors attributed the C 1*s* signal at 287.0 eV to adsorbed CO that upon heating at 300 ºC dissociates given rise to a contribution at 284.6 eV.

On studying the Boudouard reaction on Cu nanoclusters, Olmos-Asar *et al.*[48] detected C 1s components at 283.5− 283.9 eV that appear upon CO adsorption. These contributions were ascribed to adsorbed carbide species as a result of CO dissociation. Rodriguez *et al.*[43] studied the accumulation of carbon on Pt black by XPS and found the presence of a contribution at 283.5 eV on regenerated samples that they assigned to the presence of isolated carbon atoms on the platinum surface, discarding the existence of carbidic species that should appear at lower binding energies (*ca.* 282.5 eV). C 1*s* signals at 286.1 and 286.9 eV arising from CO adsorbed on two difference metallic sites. Nierhoff *et al.*[49] described CO adsorbed on Pt sites at 286.9 eV in a dynamical surface study on CuPt alloys, while Eren *et al.*[50] located adsorbed CO on Cu sites at 286.1eV. These authors[50] also related the peak at 287.9 eV to CO on Cu_2O

species. This peak assignment involves the presence of a characteristic peak in the O 1*s* region at 534.2 eV which was not detected in our work. Chung *et al.*[51] assigned a peak at 532.5 eV to CO molecules adsorbed on-top metallic sites in their study of the oxidation of CO on a Pt(110) surface.

These data suggest a Boudouard-like reaction as the main carbon removing process under CO_2 atmosphere. Once the surface is carbon free, the CO_2 gas molecules interact with the metallic surface undergoing a dissociation process that results in the formation of adsorbed CO and atomic oxygen species (529.9 eV). However, the presence of subsurface oxygen cannot be discarded as responsible for the peak at 531.6 eV.

Additionally, Figure 8 shows a HRTEM image of $PtCu_3$ nanoparticles alloy after H_2-rich atmosphere exposure confirming the presence of the carbonaceous layer that covers the catalyst while the image corresponding to $PtCu_3$ nanoparticles treated with CO_2 exhibits a free-carbon surface.

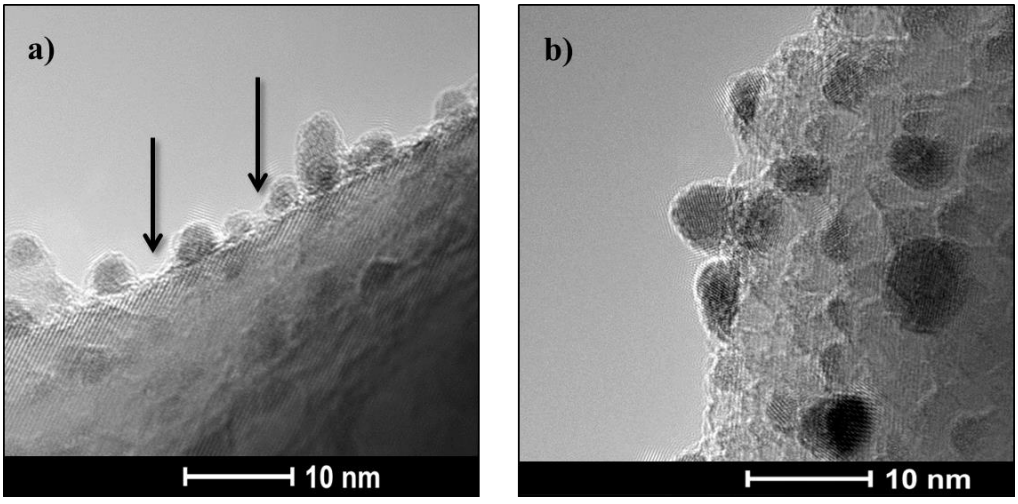

Figure 9. HRTEM images comparing: **a)** $PtCu_3$ nanoparticles alloy after H_2 treatment, **b)** $PtCu_3$ nanoparticles alloy after CO_2 treatment.

The binding energy difference as estimated from DFT calculations between subsurface and surface oxygen is in the 0.8-1.7 eV range[52]. A value of 1.7 eV has been estimated for subsurface oxygen in the silver−oxygen system[53]. Considering that

~530 eV is ascribed to surface oxygen[54] the signal at 531.6 eV could be assigned to subsurface oxygen.

Andersson *et al.*[55,56] studied the autocatalytic water dissociation on Cu (110) metal surface by APXPS and observed two different types of OH species during the exposure of the metal to 1 Torr pressure of water at different temperatures: hydroxyl species adsorbed on the metal surface (530.4 eV) and OH hydrogen-bonded to H_2O molecules (530.9 eV). Moreover, Andersson *et al.*[55] and Eren *et al.*[50] confirmed the presence of adsorbed molecular water in their respective works, reporting an O 1*s* contribution at 532.5 eV. This agrees with Favaro *et al.*[57] that suggest that O_{ads} groups on the Cu surface can serve as nucleation sites for hydroxylation, but also point out the difficulty of detecting Cu-OH groups since in the same spectral range (530.6–530.8 eV) several oxygen-based species overlap (formate, C-OH, and O-R species).

The hardly observable C 1*s* contributions, except for the CO_2 gas phase, upon CO_2 treatment discard any ascription to oxygenated hydrocarbons suggesting that the adsorbed species are the consequence of CO_2 dissociation and further interaction with the residual H_2 atmosphere in the reaction chamber (H_2 and CO are typical residual gases in UHV systems)[58]. The formation of suboxidic surface species (529.9 eV), adsorbed OH hydrogen-bonded to H_2O species (530.9 and 532.6 eV) and subsurface oxygen at 531.6 eV[59] is consistent with a reaction scheme in which carbon is removed through the Boudouard reaction, although a contribution to the signal of adsorbed CO species cannot be discarded.

After reaction a small fraction of CO may remain adsorbed but the main reaction seems to involve CO_2 dissociation giving rise to the formation of adsorbed oxygen atoms (surface suboxidic species) and subsurface oxygen atoms acting as nucleation sites for adsorbed hydroxyl species formed by interaction with the residual H_2 in the reaction chamber. The whole process may be schematized as followed equation shows:

(1.1) $C + CO_2 \leftrightharpoons 2CO$

(1.2) $CO_2 \leftrightharpoons CO\uparrow + O_{ads}$

(1.3) $H_2 \leftrightharpoons 2H_{ads}$

(1.4) $H_{ads} + O_{ads} \leftrightharpoons OH_{ads}$

(1.5) $H_{ads} + OH_{ads} \leftrightharpoons H_2O_{ads}$

Once the carbon species have been completely removed from the surface, the CO_2 was pumped out and H_2 was introduced into the reaction chamber. After replacing the gas atmosphere, differences in the nature of the adsorbed species in the O 1*s* signal are hardly observable except by a modification of their relative intensities. The component at 531.6 eV grows at the expense of the signal at 529.9 eV. However, under H_2 gas two contributions in the C 1*s* region appeared at 284.6 and 283.3 eV assigned to aromatic carbon and isolated carbon atoms adsorbed on the surface, respectively[43]. This is an indication of the dissociation of carbon oxides resulting in the formation of surface carbon. The increased electron density resulting from H_2 adsorption and dissociation helps to dissociate the carbon oxide molecules remaining in the reaction chamber. It should be remarked that the sample holder is placed inside a conventional UHV bell jar being the total volume of the reaction chamber quite big (~38 L). Prior to any experiment the sample is evacuated to ~10^{-6} mbar and therefore during the whole experiment the reactive atmosphere may contain enough residual molecules of the previous CO_2 atmosphere (~10^{-9} moles).

The above mentioned dissociation results in an increase in the oxygen of surface oxygen species but not in a change in the nature of such species. In general, there is an increase in the relative concentration of species having O 1*s* signals at 530.9 eV (OH species), 531.6 eV (subsurface oxygen) and 532.6 eV (adsorbed molecular H_2O). This is consistent with the ascriptions and mechanism proposed for the appearance of adsorbed species upon interaction with the CO_2 atmosphere.

A further treatment in a H_2+CO_2 atmosphere allows simulating the actual environment proposed for the industrial PtCu catalysts for the CO-PROX reaction[12]. In this atmosphere it is clear the absence of isolated carbon atoms or carbidic species on

the nanoparticle surface being only evident the presence of sp^2 and sp^3 carbonaceous species on the nanoparticle surface (C1*s* components at 284.6 and 285.2 eV, respectively). In addition to these contributions, there is another one appearing at 286.5 eV, which is characteristic of the presence of adsorbed carbon oxides species[41,43] and indicates that CO_2 is dissociated on the catalyst surface giving rise to adsorbed CO species and carbon sp^3 species. This dissociation process is clearly detected by the increase in the surface oxygen concentration and the presence of CO and H_2O in the gas phase signals at 535.5 and 538.0 eV, respectively. Moreover, the components at 531.6 eV (subsurface oxygen and adsorbed CO), 530.9 eV (OH) and 532.6 eV (H_2O) increase. Considering all these evidences, the following reaction scheme for the interaction of the H_2+CO_2 mixture with the clean nanoparticle surface is proposed:

(1.6) $CO_2 \leftrightharpoons CO_{2\ ads}$

(1.7) $CO_{2\ ads} \leftrightharpoons CO_{ads} + O_{ads}$

(1.8) $CO_{ads} \leftrightharpoons CO \uparrow$

(1.3) $H_2 \leftrightharpoons 2H_{ads}$

(1.4) $H_{ads} + O_{ads} \leftrightharpoons OH_{ads}$

(1.5) $H_{ads} + OH_{ads} \leftrightharpoons H_2O_{ads}$

(1.9) $H_2O_{ads} \leftrightharpoons H_2O \uparrow$

(1.10) $CO_2 + H_2 \leftrightharpoons CO + H_2O$

The effect of surface carbon overlayers is clearly seen in the catalytic behavior of the nanoparticles. The activity of the $PtCu_3$ nanoparticles in the preferential oxidation of CO was analyzed at 200ºC over samples pretreated at 350ºC either under hydrogen or CO_2 atmospheres. Figure 10 plots the turn-over-frequency (TOF) values calculated by taking account the nanoparticle average size deduced from HRTEM analysis and mathematically modeled cuboctahedral particles[60,61]. On the freshly pretreated

nanoparticles the TOF value is ca.~ 4 times higher for the carbon covered surface (H_2-pretreated) than for the clean surface. After cooling down the sample it was submitted to new reaction cycle which results in an increase in the catalytic activity that is particularly enhanced in the CO_2-pretreated sample. The CO-PROX stream ($5H_2$:$1H_2O$:$1CO_2$:0.1CO:$0.1O_2$) not only contains H_2 but H_2O and CO_2 therefore the amount of surface carbon with respect to the one preset after the H_2-pretreatment is reduced (Figure 5). On the other hand, the coexistence of H_2 and CO_2 in the feed stream should result in the formation of surface carbon. These results clearly suggest that the active surface is in fact partially covered by a carbonaceous layer.

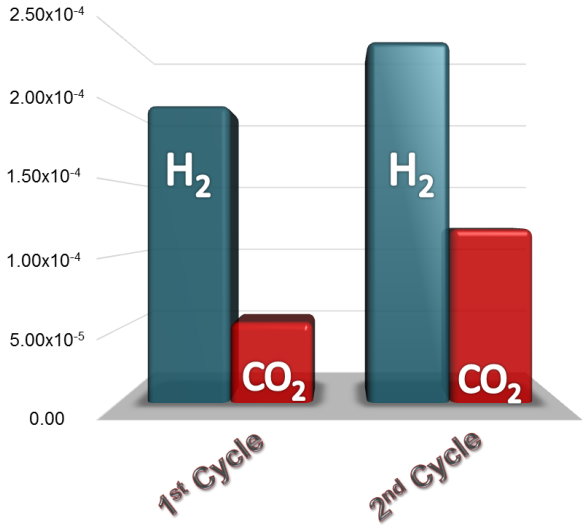

Figure 10. Effect of the surface carbon deposits on CO-PROX performance for unsupported PtCu3 nanoparticles at 200ºC. CO-PROX stream molar ratio; $5H_2$:$1H_2O$:$1CO_2$:0.1CO:$0.1O_2$.

4. CONCLUSIONS

Well-defined PtCu bimetallic alloy nanoparticles (1:3 atomic ratio) were synthesized and characterized as model catalysts for the preferential oxidation of CO. The presence of surface carbon deposits from the use of organic capping agents has been evidenced. An alternative surface cleaning method has been developed which highlights the soft conditions and the possible effects on the nature of the active surface sites. This cleaning method consists on washing the nanoparticles with an acid solution followed by an *in situ* CO_2 treatment. A set of surface reactions leading to the elimination

of carbon and the formation of subsurface oxygen species is proposed. At the steady state two main processes coexist; the formation of carbon deposits by dissociation of carbon oxides favored by the presence of adsorbed hydrogen and the elimination of carbon deposits by the Boudourad reaction. This results in a surface carbon layer partially covering the nanoparticle that modulates the catalytic activity.

Supporting information.

XRD data of the synthesized $PtCu_3$ nanoparticles; HRTEM analysis and size distribution before and after the washing step of the surface cleaning method; TPD-MS after the washing step of the nanoparticles; average size of the nanoparticles under the different exposure environments, copper species depth profiling analysis and TOF-values comparison of the $PtCu_3$ nanoparticles for CO-PROX reaction after H_2-conditioning treatment and after the surface cleaning method.

Author Information

Corresponding author:

*E-mail address: rcastillo4@us.es

*E-mail address: odrio@us.es

ORCID: 0000-0001-7790-3396

Acknowledgment

Financial support for this work has been obtained from the Spanish Ministerio de Economía y Competitividad (MINECO) (ENE2015-66975-C3-2-R) co-financed by FEDER funds from the European Union. C.E. acknowledges financial support from the Spanish government (MAT2012-38567-C02-02). The authors thank the support of ALBA

staff for the successful performance of the measurements at the CIRCE beamline of the ALBA Synchrotron Light Source.

REFERENCES

[1] R.Y. Zhong, K.Q. Sun, Y.C. Hong, B.Q. Xu, Impacts of organic stabilizers on catalysis of Au nanoparticles from colloidal preparation, ACS Catal. 4 (2014) 3982–3993. doi:10.1021/cs501161c.

[2] E. Taylor, S. Chen, J. Tao, L. Wu, Y. Zhu, J. Chen, Synthesis of Pt-Cu nanodendrites through controlled reduction kinetics for enhanced methanol electro-oxidation, ChemSusChem. 6 (2013) 1863–1867. doi:10.1002/cssc.201300527.

[3] C. Megías-Sayago, J.L. Santos, F. Ammari, M. Chenouf, S. Ivanova, M.A. Centeno, J.A. Odriozola, Influence of gold particle size in Au/C catalysts for base-free oxidation of glucose, Catal. Today. 306 (2017) 183–190. doi:10.1016/j.cattod.2017.01.007.

[4] H.L. Nguyen, L.E.M. Howard, G.W. Stinton, S.R. Giblin, B.K. Tanner, I. Terry, a. K. Hughes, I.M. Ross, A. Serres, J.S.O. Evans, Synthesis of size controlled fcc and fct FePt nanoparticles., Chem. Mater. 37 (2006) 6414–6424. doi:10.1021/cm062127e.

[5] A. Roucoux, J. Schulz, H. Patin, Reduced transition metal colloids: A novel family of reusable catalysts?, Chem. Rev. 102 (2002) 3757–3778. doi:10.1021/cr010350j.

[6] A. Quintanilla, V.C.L. Butselaar-Orthlieb, C. Kwakernaak, W.G. Sloof, M.T. Kreutzer, F. Kapteijn, Weakly bound capping agents on gold nanoparticles in catalysis: Surface poison?, J. Catal. 271 (2010) 104–114.

doi:10.1016/j.jcat.2010.02.013.

[7] L.R. Baker, G. Kennedy, J.M. Krier, M. Van Spronsen, R.M. Onorato, G.A. Somorjai, The role of an organic cap in nanoparticle catalysis: Reversible restructuring of carbonaceous material controls catalytic activity of platinum nanoparticles for ethylene hydrogenation and methanol oxidation, Catal. Letters. 142 (2012) 1286–1294. doi:10.1007/s10562-012-0904-3.

[8] J.Y. Park, C. Aliaga, J.R. Renzas, H. Lee, G.A. Somorjai, The role of organic capping layers of platinum nanoparticles in catalytic activity of CO oxidation, Catal. Letters. 129 (2009) 1–6. doi:10.1007/s10562-009-9871-8.

[9] S. Campisi, D. Ferri, A. Villa, W. Wang, D. Wang, O. Kröcher, L. Prati, Selectivity Control in Palladium Catalyzed Alcohol Oxidation Through Selective Blocking of Active Sites Selectivity Control in Palladium Catalyzed Alcohol Oxidation Through Selective Blocking of Active Sites, 120 (2016) 14027–14033. doi:10.1021/acs.jpcc.6b01549.

[10] J.A. Lopez-Sanchez, N. Dimitratos, C. Hammond, G.L. Brett, L. Kesavan, S. White, P. Miedziak, R. Tiruvalam, R.L. Jenkins, A.F. Carley, D. Knight, C.J. Kiely, G.J. Hutchings, Facile removal of stabilizer-ligands from supported gold nanoparticles, Nat. Chem. 3 (2011) 551–556. doi:10.1038/nchem.1066.

[11] M. Luo, Y. Hong, W. Yao, C. Huang, Q. Xu, Q. Wu, Facile removal of polyvinylpyrrolidone (PVP) adsorbates from Pt alloy nanoparticles, J. Mater. Chem. A. 3 (2015) 2770–2775. doi:10.1039/C4TA05250A.

[12] F. Romero-Sarria, S. Garcia-Dali, S. Palma, E.M. Jimenez-Barrera, L. Oliviero, P. Bazin, J.A. Odriozola, The role of carbon overlayers on Pt-based catalysts for H2-cleanup by CO-PROX, Surf. Sci. 648 (2015) 84–91. doi:10.1016/j.susc.2015.12.017.

[13] M. Cargnello, C. Chen, B.T. Diroll, V.V.T. Doan-Nguyen, R.J. Gorte, C.B. Murray, Efficient removal of organic ligands from supported nanocrystals by fast thermal annealing enables catalytic studies on well-defined active phases, J. Am. Chem. Soc. 137 (2015) 6906–6911. doi:10.1021/jacs.5b03333.

[14] S. Alayoglu, A.U. Nilekar, M. Mavrikakis, B. Eichhorn, Ru-Pt core-shell nanoparticles for preferential oxidation of carbon monoxide in hydrogen, Nat. Mater. 7 (2008) 333–338. doi:10.1038/nmat2156.

[15] W. Zhan, J. Wang, H. Wang, J. Zhang, X. Liu, P. Zhang, M. Chi, Y. Guo, Y. Guo, G. Lu, S. Sun, S. Dai, H. Zhu, Crystal Structural effect of AuCu lloy nanoparticles on catalytic CO Oxidation, J. Am. Chem. Soc. 139 (2017) 8846–8854. doi:10.1021/jacs.7b01784.

[16] G. Guisbiers, S. Mejia-Rosales, S. Khanal, F. Ruiz-Zepeda, R.L. Whetten, M. José-Yacaman, Gold-copper nano-alloy, " tumbaga ", in the era of nano: Phase diagram and segregation, Nano Lett. 14 (2014) 6718–6726. doi:10.1021/nl503584q.

[17] G. Avgouropoulos, T. Ioannides, C. Papadopoulou, A comparative study of Pt/gamma-Al2O3, Au/alpha-Fe2O3 and CuO–CeO2 catalysts for the selective oxidation of carbon monoxide in excess hydrogen., Catal. Today. 75 (2002) 157–167.

[18] S.K. Jain, E.M. Crabb, L.E. Smart, D. Thompsett, A.M. Steele, Environmental Controlled modification of Pt / Al 2 O 3 for the preferential oxidation of CO in hydrogen : A comparative study of modifying element, Appl. Catal. B Environ. 89 (2009) 349–355. doi:10.1016/j.apcatb.2008.12.013.

[19] V. Pérez-Dieste, L. Aballe, S. Ferrer, J. Nicolàs, C. Escudero, A. Milán, E. Pellegrin, Near ambient pressure XPS at ALBA, in: J. Phys. Conf. Ser., 2013.

doi:10.1088/1742-6596/425/7/072023.

[20] S. Tanurna, C.J. Powell, D.R. Penn, Calculations of Electron Inelastic Mean Free Paths, Surf. Interface Anal. 17 (1991) 927–939. doi:10.1002/sia.740171305.

[21] M. Neergat, R. Rahul, Unsupported Cu-Pt Core-Shell Nanoparticles: Oxygen Reduction Reaction (ORR) Catalyst with Better Activity and Reduced Precious Metal Content, J. Electrochem. Soc. 159 (2012) 234–241. doi:10.1149/2.039207jes.

[22] Y.K. Du, P. Yang, Z.G. Mou, N.P. Hua, L. Jiang, Thermal decomposition behaviors of PVP coated on platinum nanoparticles, J. Appl. Polym. Sci. 99 (2006) 23–26. doi:10.1002/app.21886.

[23] Y. Borodko, H. Sook Lee, S. Hoon Joo, Y. Zhang, G. Somorjai, Spectroscopic Study of the Thermal Degradation of PVP-Capped Rh and Pt Nanoparticles in H 2 and O 2 Environments, J. Phys. Chem. C. 114 (2010) 1117–1126. doi:10.1021/jp909008z.

[24] W. Ruettinger, X. Liu, R.J. Farrauto, Mechanism of aging for a Pt / CeO 2 -ZrO 2 water gas shift catalyst, Appl. Catal. B Environ. 65 (2006) 135–141. doi:10.1016/j.apcatb.2006.01.005.

[25] O. Muller, R. Roy, Two new ternary copper-platinum oxides., J. Less-Common Met. 19 (1969) 209–214.

[26] G. Olivo, A. Barbieri, V. Dantignana, F. Sessa, V. Migliorati, M. Monte, S. Pascarelli, T. Narayanan, O. Lanzalunga, S. Di Stefano, P.D. Angelo, Following a Chemical Reaction on the Millisecond Time Scale by, J. Phys. Chem. Lett. 8 (2017) 2958–2963. doi:10.1021/acs.jpclett.7b01133.

[27] C.H. Bamford, M.J.S. Dewar, The Thermal Decomposition of Acetic Acid, J Am

Chem Soc. 0 (1949) 2877–2882.

[28] L. Shore, W. F.Ruettinger, R.J. Farrauto, Platinum group metal promoted copper oxidation catalysts and methods for carbon monoxide remediation., US 6,913,739 B2, 2005.

[29] G. Moretti, The Wagner plot and the Auger parameter as tools to separate initial- and final-state contributions in X-ray photoemission spectroscopy, Surf. Sci. 618 (2013) 3–11. doi:10.1016/j.susc.2013.09.009.

[30] T.H. Fleisch, G.J. Mains, Reduction of copper oxides by UV radiation and atomic hydrogen studied by XPS, Appl. Surf. Sci. 10 (1982) 51–62. doi:10.1016/0378-5963(82)90134-9.

[31] G. Moretti, Auger parameter and Wagner plot in the characterization of chemical statesby X-ray photoelectron spectroscopy: a review, J. Electron Spectros. Relat. Phenomena. 95 (1998) 95–144.

[32] S. Poulston, P.M. Parlett, P. Stone, M. Bowker, Surface oxidation and reduction of CuO and Cu2O studied using XPS and XAES, Surf. Interface Anal. 24 (1996) 811–820. doi:10.1002/(SICI)1096-9918(199611)24:12<811::AID-SIA191>3.0.CO;2-Z.

[33] G. Moretti, A. Palma, E. Paparazzo, M. Satta, Auger parameter and Wagner plot studies of small copper clusters, Surf. Sci. 646 (2016) 298–305. doi:10.1016/j.susc.2015.07.018.

[34] E.D. Roberts, P. Weightman, C.E. Johnson, Auger vacancy satellite structure in the L3M4,5M4,5 Auger spectra of copper, J. Phys. Chem. C. 8 (1975) 301–304.

[35] E. Antonides, E.C. Janse, G.A. Sawatzky, LMM Auger-Spectra of Cu, Zn, Ga, and Ge .1. Transition-Probabilities, Term Splittings, and Effective Coulomb Interaction, Phys. Rev. B. 15 (1977) 1669–1679.

doi:10.1103/PhysRevB.15.1669.

[36] N. Pauly, S. Tougaard, F. Yubero, LMM Auger primary excitation spectra of copper, Surf. Sci. 630 (2014) 294–299. doi:10.1016/j.susc.2014.08.029.

[37] G. Schön, ESCA studies of Cu, Cu2O and CuO, Surf. Sci. 35 (1973) 96–108. doi:10.1016/0039-6028(73)90206-9.

[38] H. He, J. Klinowski, M. Forster, A. Lerf, A new structural model for graphite oxide, Chem. Phys. Lett. 287 (1998) 53–56. https://es.wikipedia.org/wiki/Óxido_de_grafito.

[39] C. Petit, M. Seredych, T.J. Bandosz, Revisiting the chemistry of graphite oxides and its effect on ammonia adsorption, J. Mater. Chem. 19 (2009) 9176–9185. doi:10.1039/b916672f.

[40] D.S. Jensen, S.S. Kanyal, N. Madaan, A.J. Miles, R.C. Davis, R. Vanfleet, M.A. Vail, A.E. Dadson, M.R. Linford, Ozone priming of patterned carbon nanotube forests for subsequent atomic layer deposition-like deposition of SiO 2 for the preparation of microfabricated thin layer chromatography plates, J. Vac. Sci. Technol. B. 31 (2013) 031803. doi:10.1116/1.4801834.

[41] S. Drewniak, R. Muzyka, A. Stolarczyk, T. Pustelny, M. Kotyczka-Morańska, M. Setkiewicz, Studies of reduced graphene oxide and graphite oxide in the aspect of their possible application in gas sensors, Sensors. 16 (2016) 1–16. doi:10.3390/s16010103.

[42] S. Obata, H. Tanaka, K. Saiki, Electrical and spectroscopic investigations on the reduction mechanism og graphene oxide, Carbon N. Y. 55 (2013) 126–132. doi:10.1016/j.carbon.2012.12.018.

[43] N.M. Rodriguez, P.E. Anderson, A. Wootsch, Z. Paál, U. Wild, R. Schlögl, Z. Paál, XPS, EM, and catalytic studies of the accumulation of carbon on Pt black,

J. Catal. 197 (2001) 365–377. doi:10.1006/jcat.2000.3081.

[44] X. Fan, C. Yu, J. Yang, Z. Ling, J. Qiu, Hydrothermal synthesis and activation of graphene-incorporated nitrogen-rich carbon composite for high-performance supercapaitors, Carbon N. Y. 70 (2014) 130–141. doi:10.1016/j.carbon.2013.12.081.

[45] B. Eren, H. Kersell, R.S. Weatherup, C. Heine, E.J. Crumlin, C.M. Friend, M.B. Salmeron, Structure of the Clean and Oxygen-Covered Cu(100) Surface at Room Temperature in the Presence of Methanol Vapor in the 10-200 mTorr Pressure Range, J. Phys. Chem. B. 122 (2018) 548–554. doi:10.1021/acs.jpcb.7b04681.

[46] Z. Liu, T. Duchoň, H. Wang, E.W. Peterson, Y. Zhou, S. Luo, J. Zhou, V. Matolín, D.J. Stacchiola, J.A. Rodriguez, S.D. Senanayake, Mechanistic Insights of Ethanol Steam Reforming over Ni-CeOx (111): The Importance of Hydroxyl Groups for Suppressing Coke Formation, J. Phys. Chem. C. 119 (2015) 18248–18256. doi:10.1021/acs.jpcc.5b04310.

[47] J.P. Simonovis, A. Hunt, R.M. Palomino, S.D. Senanayake, I. Waluyo, Enhanced Stability of Pt-Cu Single-Atom Alloy Catalysts : In Situ Characterization of the Pt / Cu (111) Surface in an Ambient Pressure of CO, J. Phys. Chem. C. 122 (2018) 4488–4495. doi:10.1021/acs.jpcc.8b00078.

[48] J.A. Olmos-Asar, E. Monachino, C. Dri, A. Peronio, C. Africh, P. Lacovig, G. Comelli, A. Baldereschi, M. Peressi, E. Vesselli, CO on supported Cu nanoclusters: Coverage and finite size contributions to the formation of carbide via the boudouard process, ACS Catal. 5 (2015) 2719–2726. doi:10.1021/cs501361h.

[49] A. Nierhoff, C. Conradsen, D. McCarthy, T.P. Johansson, J. Knudsen, I.

Chorkendorff, Adsorbate induced surface alloy formation investigated by near ambient pressure X-ray photoelectron spectroscopy, Catal. Today. 244 (2015) 130–135. doi:10.1016/j.cattod.2014.06.024.

[50] B. Eren, C. Heine, H. Bluhm, G.A. Somorjai, M. Salmeron, Catalyst Chemical State during CO Oxidation Reaction on Cu(111) Studied with Ambient-Pressure X-ray Photoelectron Spectroscopy and Near Edge X-ray Adsorption Fine Structure Spectroscopy, J. Am. Chem. Soc. 137 (2015) 11186–11190. doi:10.1021/jacs.5b07451.

[51] J. Chung, F. Aksoy, M.E. Grass, H. Kondoh, P. Ross, Z. Liu, B. Simon, Surface Science In-situ study of the catalytic oxidation of CO on a Pt (1 1 0) surface using ambient pressure X-ray photoelectron spectroscopy, Surf. Sci. 603 (2009) L35–L38. doi:10.1016/j.susc.2009.01.016.

[52] A. Eilert, F. Cavalca, F.S. Roberts, J. Osterwalder, C. Liu, M. Favaro, E.J. Crumlin, H. Ogasawara, D. Friebel, L.G.M. Pettersson, A. Nilsson, Subsurface Oxygen in Oxide-Derived Copper Electrocatalysts for Carbon Dioxide Reduction, J. Phys. Chem. Lett. 8 (2017) 285–290. doi:10.1021/acs.jpclett.6b02273.

[53] T.C.R. Rocha, A. Oestereich, D. V Demidov, M. Hävecker, S. Zafeiratos, G. Weinberg, V.I. Bukhtiyarov, A. Knop-Gericke, R. Schlögl, The silver – oxygen system in catalysis : new insights by near ambient pressure X-ray photoelectron spectroscopy, Phys. Chem. Chem. Phys. 14 (2012) 4554–4564. doi:10.1039/c2cp22472k.

[54] H. Tillborg, A. Nilsson, B. Hernnäs, N. Mårtensson, R.E. Palmer, X-ray and UV photoemission studies of mono- , bi- and multilayers of physisorbed molecules : 0 , and N , on graphite, Surf. Sci. 295 (1993) 1–12.

[55] K. Andersson, G. Ketteler, H. Bluhm, S. Yamamoto, H. Ogasawara, L.G.M.

Pettersson, M. Salmeron, A. Nilsson, Autocatalytic Water Dissociation on Cu (110) at Near Ambient Conditions, J Am Chem Soc. 130 (2008) 2793–2797. doi:10.1021/ja073727x.

[56] K. Andersson, G. Ketteler, H. Bluhm, S. Yamamoto, H. Ogasawara, L.G.M. Pettersson, M. Salmeron, A. Nilsson, Bridging the Pressure Gap in Water and Hydroxyl Chemistry on Metal Surfaces : The Cu (110) Case, J. Phys. Chem. C. 111 (2007) 14493–14499. doi:10.1021/jp073681u.

[57] M. Favaro, H. Xiao, T. Cheng, W.A. Goddard, J. Yano, E.J. Crumlin, Subsurface oxide plays a critical role in CO 2 activation by Cu (111) surfaces to form chemisorbed CO 2 , the first step in reduction of CO 2, Proc. Natl. Acad. Sci. U. S. A. (2017) 1–6. doi:10.1073/pnas.1701405114.

[58] T.J. Gay, J.A. Brand, M.C. Fritts, J.E. Furst, M.A. Khakoo, E.R. Mell, M.T. Sieger, W.M.K.P. Wijayaratna, Clean ultrahigh vacuum system with single-structure diffusion pumps, J. Vac. Sci. Technol. 12 (1994) 2903–2910.

[59] X. Deng, A. Verdaguer, T. Herranz, C. Weis, H. Bluhm, M. Salmeron, Surface Chemistry of Cu in the presence of CO2 and H2O, Langmuir. 24 (2008) 9474–9478.

[60] R. Van Hardeveld, F. Hartog, The statistics of surface atoms and surface sites on metal crystals, Surf. Sci. 15 (1969) 189–230. doi:10.1016/0039-6028(69)90148-4.

[61] S. Ivanova, V. Pitchon, C. Petit, Application of the direct exchange method in the preparation of gold catalysts supported on different oxide materials, J. Mol. Catal. A Chem. 256 (2006) 278–283. doi:10.1016/j.molcata.2006.05.006.

TOC Graphic

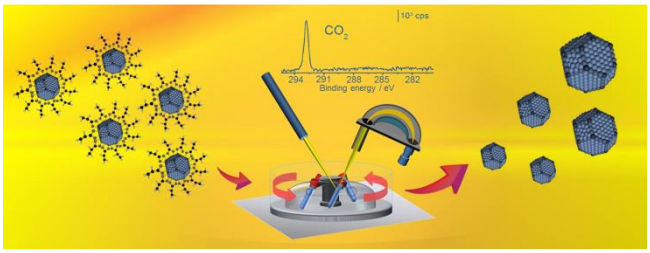
10³ cps
CO2
294
291
288
285
282
Binding energy / eV